LAWRENCE
LIVERMORE
NATIONAL
LABORATORY

LLNL-TR-676885

Validating Laser-Induced Birefringence Theory with Plasma Interferometry

C. Chen

September 2, 2015

Disclaimer

This work performed under the auspices of the U.S. Department of Energy by Lawrence Livermore National Laboratory under Contract DE-AC52-07NA27344.

Validating laser-induced birefringence theory with plasma interferometry

Cecilia Chen

Science Undergraduate Laboratory Internship (SULI)

U.S. Department of Energy, Office of Science

Cornell University

Lawrence Livermore National Laboratory

Livermore, California

August 4, 2015

Prepared in partial fulfillment of the requirements of the Science Undergraduate Laboratory Internship (SULI) program managed by the U.S. Department of Energy, Office of Science. Completed under the direction of David Turnbull in the National Ignition Facility (NIF) & Photon Science Directorate at Lawrence Livermore National Laboratory.

ABSTRACT

Validating laser-induced birefringence theory with plasma interferometry. CECILIA CHEN (Cornell University, Ithaca, NY 14853). DAVID TURNBULL, CLEMENT GOYON, BRAD POLLOCK, and PIERRE MICHEL (Lawrence Livermore National Laboratory, Livermore, CA 94550).

Intense laser beams crossing paths in plasma is theorized to induce birefringence in the medium, resulting from density and refractive index modulations that affect the polarization of incoming light. The goal of the associated experiment, conducted on Janus at Lawrence Livermore's Jupiter Laser Facility, was to create a tunable laser-plasma waveplate to verify the relationship between dephasing angle and beam intensity, plasma density, plasma temperature, and interaction length. Interferometry analysis of the plasma channel was performed to obtain a density map and to constrain temperature measured from Thomson scattering. Various analysis techniques, including Fast Fourier transform (FFT) and two variations of fringe-counting, were tried because interferograms captured in this experiment contained unusual features such as fringe discontinuity at channel edges, saddle points, and islands. The chosen method is flexible, semi-automated, and uses a fringe tracking algorithm on a reduced image of pre-traced synthetic fringes. Ultimately, a maximum dephasing angle of 49.6° was achieved using a 1200 μm interaction length, and the experimental results appear to agree with predictions.

INTRODUCTION

A waveplate is an optical device that rotates the polarization, or electric field orientation, of light passing through it. Waveplates are made from birefringent materials, which are materials that have different indices of refraction along different axes. Conventional waveplates are made from birefringent crystals such as calcite, but any birefringent material will have the properties necessary to alter the polarization of incoming light.

This experiment pursued the creation of a tunable laser-plasma waveplate on the basis of polarization control mechanisms theorized by Michel *et al.*[1] Laser beams crossing paths in plasma produce spatial modulations in plasma density, which translates to spatial modulations in the plasma's refractive index. The key to plasma birefringence rests with the initial polarizations of the two beams shown in Figure 1: only the polarization component(s) common to both beams can interact. A stationary "beat wave" forms along that axis, effectively making it the slow axis in a birefringent material. In this experiment, the high-intensity, gas-ionizing pump beam is horizontally polarized while the probe beam is initially elliptically polarized at an axis angle of 41° and a starting dephasing angle of 49°.[2,3] The laser-plasma waveplate acts upon the probe beam by retarding its horizontal polarization component relative to the vertical.

The amount of phase delay imparted by the waveplate between horizontal and vertical components of a wave's polarization is quantified by the dephasing angle. All following mentions of dephasing angle will refer to changes from the initial angle of 49°:

$$\delta \propto \frac{n_e I_0 L}{T_e} \tag{1}$$

where n_e is the plasma electron density, I_0 is the incident intensity of the pump laser, L is the interaction length between the pump and probe beams, and T_e is the plasma electron temperature. The goal of the experiment is to verify the theory through adjusting the above four parameters

and demonstrating control over polarization change in the probe beam. In particular, density and temperature were the most variable while intensity and interaction length changed neither significantly nor often.

This paper will focus on spatial density measurements using interferometry of the plasma channel. Density information is crucial for verification of the theory because dephasing angle depends on density. Furthermore, the diagnostic responsible for determining plasma temperature, another parameter controlling dephasing angle, cannot give accurate temperature unless density is known to some degree of certainty. Obtaining accurate measurements of temperature and density is the foundation for calculating predicted dephasing angles, which ultimately serves to verify the theory through comparison of experimental and predicted values.

THE EXPERIMENT

The experiment was carried out in the Janus target area of the Jupiter Laser Facility at Lawrence Livermore National Laboratory (LLNL). A sketch of the experimental setup and diagnostics placement can be found in Figure 2. Both the pump and probe beams are seeded off the same 1053 nm laser and are aimed at an angle of 27° toward each other. The pump beam is named for its role in ionizing gas to form plasma, and the probe beam is subjected to polarization changes caused by intersecting the pump beam in plasma. For the majority of the shots, a 600 μm phase plate was used to give the pump a uniform intensity distribution across a 600 μm beam diameter. (A few shots were later done using a 1000 μm phase plate to verify that a longer interaction length leads to greater dephasing, given that the other parameters remained constant.) The probe beam maintained a 100 μm-diameter Gaussian intensity profile throughout the experiment. In a single shot sequence, the gas jet is first triggered to release a puff of helium gas

at a preset back pressure at target chamber center (TCC) in the vacuum target chamber. Next, the early portion of the pump beam pushes through the gas to ionize it into plasma. Approximately 2 ns later, the probe beam intersects with the pump beam, which at this point is just acting as a regular beam propagating through plasma, and experiences a change in polarization due to the laser-plasma waveplate.

Diagnostics

Four diagnostics were employed to measure the plasma electron density, plasma electron temperature, incident pump beam intensity, and change in probe beam polarization:

- Probe polarization (primary diagnostic)
- Interferometry – spatial n_e variation
- Thomson scattering – T_e and n_e at TCC
- Incident and transmitted pump signals – I_0

Probe polarization

The polarization diagnostic uses a Wollaston prism to decompose the transmitted probe polarization into two orthogonal components that travel along separate beam paths. The incident polarization stays constant and is known from a calibrating shot through vacuum. Changes in probe polarization are detected by changes in the ratio of vertical to horizontal polarization components (Figure 3).

Interferometry

A Mach-Zehnder interferometer, depicted in Figure 4, was modified for use in the experiment. Instead of splitting a single beam into two parts, having each beam travel through a different leg, and recombining them to form an interference pattern, a single, 1 cm-wide Hidra beam was used to image the plasma interferogram. Because the Hidra cross section is much

larger than the plasma channel, the beam can be folded to interfere the portion that travelled through the plasma with the part that remained in vacuum. Hidra is co-timed with the probe beam to capture the plasma conditions at the moment of interaction between the pump and probe. The interferogram is captured by a CCD camera, and the displacement of the fringes can be analyzed to extract density information in the plasma.

Thomson scattering

Thomson scattering collects light scattered vertically in the target chamber off of the pump beam, collimates it, and sends it through a spectrometer and streak camera to resolve the data in wavelength and time. It produces data that is dependent on both plasma density and temperature. As a result, this diagnostic is coupled with interferometry, which gives spatial density gradients within the plasma, in order to constrain the range of possible plasma temperatures.

Incident and transmitted pump signals

This diagnostic generates time-resolved waveforms of pump beam power (and therefore intensity). The incident pump intensity at the time of probe beam interaction can be gathered from the waveforms.

METHODS OF INTERFEROMETRY ANALYSIS

Interferograms of the plasma channel convey information about density variation in space through fringe shape and spacing. Several analysis techniques were tried on relatively well-defined interferograms such as the one in Figure 5(a) to find the most appropriate, robust, and successful technique for the set of experimental images. The fringe-counting approach on fringe

traces produced the best results. Afterwards, a density map was produced from a phase shift map using a method independent of the approach chosen to find phase shift.

Mapping phase shift

The phase shift at a particular point (h,z), where h is the height along the pump beam, z is the distance along the beam path, and (0,0) marks TCC, is given by the number of fringes the point has shifted away from its reference fringe multiplied by 2π. A single fringe shift from crest to crest (bright fringe to bright fringe) or trough to trough (dark fringe to dark fringe) represents one period; the 2π factor exists merely to convert fringe shift to phase shift in units of radians. Phase shift will be denoted as $\Delta\phi$ while fringe shift will be written as $\Delta\phi_N$. Reference fringes, marked in Figure 6(a), are traces of what the interferogram would look like if no plasma were present. Note that phase shift values are pinned to the deformed fringe coordinates and not the reference coordinates. This is because the light forming the fringes themselves hit fixed points on the CCD matrix and are not displaced with the reference fringes as they undergo phase shifting.

Fast Fourier transform (FFT)

The fastest and most automated method for interferogram analysis utilizes a 2D Fast Fourier transform to determine spatial phase components in an image. In general terms, the FFT method considers each row and column in the image, represents the grayscale oscillation in pixel values between white and black as a sinusoid, and reduces the information to a map of complex values. Signals about the carrier frequency are then extracted and put through a 2D Inverse fast Fourier transform (IFFT) to reconstruct the signal and generate a phase map from another set of complex values. However, this technique did not work on the interferograms from this experiment because of discontinuities in the plasma channel edge shown in Figure 5(a). This feature is caused by a gradient of higher gas and plasma density closer to the gas jet; the fringes

are displaced so far at the plasma channel edge that they appear to "jump." Refer to Takeda *et al.*[4] for a complete description of the theory and approach.

Fringe-counting on scattered points

A manual method for obtaining phase shift was attempted for its flexibility compared to the FFT approach, since automated image processing algorithms have difficulty dealing with discontinuities that humans can visually stitch together. Figure 7 shows the scattered points and fringe shifts that were obtained by hand. This method uses substantial interpolation to fill in information for missing data points, and the choice of interpolation method appeared to greatly affect the phase shift and density maps. Consequently, an improvement on this method was sought.

Fringe-counting on fringe traces

Because fringe-counting on scattered points was incredibly tedious and could produce significant variation in plasma density based on the choice of interpolation method, more data points needed to be obtained more efficiently. The raw interferogram was first imported into GNU Image Manipulation Program (GIMP) and enlarged from 512×512 to 2048×2048 pixels at 300 pixels per inch along the x- and y-axis; no resolution was lost because the tool utilized cubic spline interpolation. Then, each fringe was traced manually on a transparent layer with the spline fit tool, making sure to resolve the discontinuity issue. Enlarging the image was a crucial step here because steep fringe slopes near the plasma channel edge may cause the fringes to bunch together and be indistinguishable from one another for a later step involving automated fringe tracking. The fringe traces were stroked with a 2 pixel-wide tip at 100% hardness and saved as a PNG file with no anti-aliasing applied. The image is then opened in MATLAB to turn any remaining grayscale pixels to black and to crop out the whitespace and leave just the fringes. It

undergoes a final touchup in Microsoft Paint to smooth out any glaring lumps and gaps that remained from the conversion of vector-based splines to a raster format.

After the pre-processing steps, the image was put through a program to generate a phase shift map:

1. The user selects the `heads` and `tails` of the fringes by clicking on the image. This information is stored in an array for indexed access.

2. A structure array, `fringes`, is created to hold information about each fringe. Each fringe has its own entry in the structure array and contains the following array fields:
   - `x` (x-coordinates of pixels belonging to the fringe)
   - `y` (y-coordinates of pixels belonging to the fringe)
   - `smoothx` (x-coordinates of fringe pixels after running 3-point smoothing)
   - `smoothy` (y-coordinates of fringe pixels after running 3-point smoothing)
   - `refx` (x-coordinates of the reference fringe)
   - `refy` (y-coordinates of the reference fringe)
   - `Nphi` (number of fringe shifts associated with the corresponding point on the fringe)

3. A fringe tracking algorithm locates points along each fringe by looking for the next pixel along the path that help it progress from head to tail.

4. The coordinates along the reference fringes are generated by linear interpolation between the first and last points along the fringe. A single y-coordinate was not used because the interferogram was slightly tilted. If the interferogram were straight and the image was taken at an angle, the whole image could just be rotated, but this was not the case.

5. A 3-point running average filter is applied to the array of raw x- and y-coordinates because the algorithm doesn't reproduce the exact raster curves. Oscillations between two pixel heights are common.

6. Fringe shift is found by finding the difference in height at a particular x-coordinate between the fringe and its reference, then dividing by the average pixel spacing between reference fringes. The reference fringes were very evenly spaced, so local spacing was not needed.

7. Fringe shift is converted to phase shift by multiplying by 2π.

The fringe tracking algorithm deserves a more detailed explanation. For each fringe in the image:

1. The algorithm begins at the selected coordinate stored in `heads` and keeps searching for the next pixel in its path, stepping along the fringe until it reaches the tail. If the selected point is not along the fringe (slight human pointing error), the code will look for the nearest black pixel and start there.

2. The current coordinate is stored in variables `currentx` and `currenty`.

3. `reach = 1` by default. It represents the neighborhood about the current coordinate that is searched for potential next moves.

4. A scalar structure is created to keep track of the 16 most recent pixels the code has tried to access (but not necessarily stored in `fringes`, which only takes pixels confirmed to be on the pre-traced fringe path). It stores the x- and y-coordinates and the priority of the attempted move relative to the previously accessed coordinate.

5. `online` is a structure that holds pixels which have potential to be the next location to move to during fringe tracking.

6. Pixels surrounding the current coordinate are assigned names 1 through 8:

```
% |-----|-----|-----|
% |  8  |  5  |  4  |
% |-----|-----|-----|
% |  7  |  x  |  1  |
% |-----|-----|-----|
% |  6  |  3  |  2  |
% |-----|-----|-----|
```

   The black pixels are added to `online` for further consideration. If none qualify, `reach` is incremented to search a larger region. The preceding steps are repeated.

7. The image is partitioned into 4 sections based on the primary direction of movement needed to make progress. These boundaries are hardcoded and need to be adjusted for each interferogram. For example, at a current coordinate on the flat, leftmost region of a fringe, the primary direction is to the right. Its U-shaped search region would be marked as:

```
% |-----|-----|-----|
% |     |  o  |  o  |
% |-----|-----|-----|
% |     |  x  |  o  |
% |-----|-----|-----|
% |     |  o  |  o  |
% |-----|-----|-----|
```

   Now, only black pixels falling within the current coordinate's search

region are kept in `online`, which gives the collection of all possible moves.

8. The median of the coordinates in `online` is calculated. Entries in `online` are sorted by their proximity to this reference coordinate.
9. Check if the current coordinate has been accessed recently. If it has, choose a different move in `online` by selecting the next unaccessed coordinate in the sorted list. Otherwise, just take the first entry. If the list has been exhausted, try again after expanding the search region.
10. After successfully finding the next move and its coordinate, save the current coordinate in `fringes`. Finally, update `currentx` and `currenty` to make the move. Restore all flags and tracking variables.

Finally, phase shift information for the remaining points in the plasma channel was found using MATLAB `griddata`'s natural neighbor interpolation. Potential interpolation methods were carefully selected considering the physical based on features specific to images obtained from the experiment and what the data representation. Desired properties include locality, since fringe deformation at a point is caused by nearby plasma; preservation of sampled points; and ideally, C^2 continuity, although C^1 is also acceptable. See Table 2 for a comparison of the interpolation methods considered: natural neighbor, cubic, and biharmonic spline. Biharmonic spline was eliminated first because it has difficulty handling large data sets and crashed when analyzing fringe data for a typical interferogram containing more than 20,000 points. Natural neighbor and cubic interpolation produced nearly identical results, but natural neighbor was chosen because it produced a slightly smoother curve.

Mapping density from phase shift

Typically, density within a 3D volume is found using an Abel inversion. However, it requires the plasma channel to be radially symmetric in both space and density, and the latter condition was not satisfied. So, only a 2D projection of average density could be obtained with

the given diagnostics. Eq. (2) is applied to the phase shift map to find average density at the projected point:

$$n_e(h,z) = \frac{\Delta\phi_N(h,z) \cdot 2n_{crit} \cdot \lambda_{laser}}{chord_{plasma}(h,z)} \quad (2)$$

$chord_{plasma}(h,z)$ is the depth of the projected plasma channel at that point. Because the channel edges fall off gradually, a modified moving-FWHM procedure was used on the phase map to find the "diameter," or distance between channel boundaries, associated with the given point. For example, if the phase shift at point (204,300) is 6 radians, the boundaries would be at coordinates about (204,300) that have a phase shift as close to 3 radians as possible. Determination of the chord length is trivial once the diameter is known.

Density gradients along the interaction length: Trends in density with energy and gas pressure

Interferograms become increasingly difficult to analyze as the gas jet back pressure and incident pump intensity increase. As shown Figure 5, the plasma channel edges become more vertical and the individual fringes within the body of the plasma also become less defined. Shots done at lower energies and lower pressures produced the best images and were best suited for the full interferogram analysis technique discussed above. Therefore, it was necessary to find trends in plasma density as a function of both gas jet back pressure and pump beam intensity (or energy, as analysis was done on the primary data set that utilized a 600 μm phase plate for the pump beam) in order to extrapolate density information for shots that produced poorly-defined interferograms. Shots with varying pressure at 300 J and shots with varying energy at 150 psi were analyzed along the interaction length outlined in Figure 6(a). Instead of obtaining a full density map for these shots, phase shifts along the TCC axis were found for fringes falling within

the box outlining the interaction region. Plasma thicknesses, or "diameters," were approximated in a consistent manner using the plasma channel edges to maintain the validity of comparisons.

Density gradients along the pump beam height: Supplementing Thomson scattering

Density gradients along the beam height also provide important information for plasma characterization. Thomson scattering collects density and temperature data from a volume rather than from a single point (Figure 8). Interferometry supplements this by providing a density gradient along the beam height. It serves as a guideline for fitting the experimental data by adjusting density and temperature parameters. Density information is taken from a lineout of the density map through TCC. Thomson scattering data analysis and parameter fitting was carried out by a colleague, Clement Goyon.

RESULTS

Mapping density from an interferogram

A sample of outputs from the interferogram analysis process—from raw image to density map—is shown in Figure 6. The full procedure is only feasible for well-defined interferograms (see Figure 5 for descriptions of features that hinder the analysis), although it can be applied to images with islands and saddle points (Figures 5(b)-(c)) after slight modifications that account for peculiar fringe orders.

Density gradients along the interaction length: Trends in density with energy and gas pressure

See Figure 9 for density variation at a fixed pressure and Figure 10 for variation at a fixed energy.

Density gradients along the pump beam height: Supplementing Thomson scattering

Figure 11 shows the density gradient for Shot 70 along the pump beam height. The minimum and maximum densities are the points of interest for constraining temperature from Thomson scattering. Figure 12 follows up by comparing the best fits to the data both before and after taking the density gradient into account.

CONCLUSIONS

This experiment tested the theory of laser-induced plasma birefringence through the creation of a plasma waveplate. The analysis detailed in this paper focused on analyzing plasma interferograms to find density, a parameter important not only for its role in calculating dephasing angle, but also for its importance in helping to determine plasma temperature, another key parameter. The main challenge faced was the presence of unusual features in the interferograms caused by a density gradient from the gas jet, illustrated in Figure 6. To work around this problem, three methods of extracting phase shift from interferograms were tried and the compromise between the two extremes was chosen.

Once a density map was produced, spatial density variations about TCC were analyzed to extract more meaningful information. A look at how density changes with gas jet back pressure concluded that density increased roughly linearly with increasing pressure, and an examination of density change with pump beam intensity concluded that density decreases with increasing energy because of faster plasma channel expansion. Using density to constrain temperature also yielded positive results. A much closer fit of the experimental data was achieved when a density range was taken into account.[5]

Validation of the theory and ongoing work

Knowledge of the plasma density and temperature, incident pump intensity, and beam interaction length can be unified to compare theoretical and experimental dephasing angles. Figure 13 shows the correlation between experimental and theoretical dephasing for 150 psi shots using a 600 μm phase plate. There is a systematic offset from the ideal line of fit, but the trend otherwise agrees within the tested range of dephasing angles. Data analysis is still ongoing, and the team is attempting to figure out why the predicted dephasing is higher. Likely reasons include underestimated intensities because of a faulty phase plate or significant timing jitter in the two beams or an underestimated density from overestimated plasma depths. The plateauing in the observed dephasing angle at higher intensities and pressures is tentatively suspected to be caused by filamentation, although this is also currently being investigated. The maximum dephasing angle achieved with a 600 μm phase plate was 49.6°.[2]

While Eq. (1) relates the dephasing angle to five different parameters, only four were varied in the main shots. The fifth, interaction length, was briefly adjusted during the last few shots. Preliminary analysis of the 1000 μm phase plate data set established a maximum dephasing angle of 48.9°.[2] Upon first glance, this is lower than that of the 600 μm phase plate, but the dephasing angles for the 1000 μm set were indeed greater for comparable intensities.[2]

Applications of a tunable laser-plasma waveplate

A laser-plasma waveplate has several advantages over conventional waveplates. First, the birefringent material is plasma, which is already in a "broken" state of matter, so it is immune to damage from high-power lasers unlike a solid, structured crystal.[3] This translates to time and cost savings from eliminating the need to perform frequent and tedious inspections of the optics, and in the case of discovered damage, replacement components. Second, the materials necessary to create a laser-plasma waveplate—a pump and probe beam, gas jet, and vacuum chamber—

already exist in most plasma experiments or can be easily integrated, thus strengthening its potential to be used as a polarization-based plasma diagnostic.[2]

ACKNOWLEDGMENTS

This experiment was conducted at the Jupiter Laser Facility at LLNL. I am grateful to Pierre Michel for finding me this opportunity to engage in experimental applied physics, particularly in my main area of interest, photonics. I would like to thank my mentors and collaborators, David Turnbull, Brad Pollock, Clement Goyon, and Pierre Michel for their wisdom and guidance, as well as my co-workers in the High Energy Density Science & Technology Division. I also appreciate the help of George Swadling, Jaebum Park, and G. Elijah Kemp in sharing their knowledge about various interferometry analysis techniques. Finally, I thank the U.S. Department of Energy, Office of Science and the SULI program for helping me realize my goal of working at NIF and learning from some of the best scientists in the field.

REFERENCES

[1]P. Michel, L. Divol, D. Turnbull, and J. D. Moody, Phys. Rev. Lett. **113**, 205001 (2014).

[2]D. Turnbull (private communication).

[3]P. Michel (private communication).

[4]Mitsuo Takeda, Hideki Ina, and Seiji Kobayashi, "Fourier-transform method of fringe-pattern analysis for computer-based topography and interferometry," J. Opt. Soc. Am. 72, 156-160 (1982).

[5]C. Goyon (private communication).

[6]P. D. Dumitru, M. Plopeanu, and D. Badea, Proceedings of the 1st European Conference of Geodesy & Geomatics Engineering, Antalya, 2013, edited by A. Badea, F. R. Ribeiro, C. Grecea, and I. Veres, Vol. 17, p. 45-52.

[7]R. Hemsley, *Interpolation on a Magnetic Field*, WWW Document, (interpolate3d.googlecode.com/files/Report.pdf).

[8]I. Amidror, "Scattered data interpolation methods for electronic imaging systems: a survey," J. Electron. Imaging. 11(2), 157-176 (2002).

[9]M. Dressler, *Art of Surface Interpolation*, WWW Document, (http://m.dressler.sweb.cz/AOSIM.pdf).

TABLES

Shot #	Pump energy (J)	Pressure (psi)	Shot #	Pump energy (J)	Pressure (psi)
42	586	150	**62**	255.4	900
44	294.1	150	**63**	165.1	900
45	154.8	150	**64**	336.6	900
47	470.3	150	**65**	341	300
48	150.7	300	**66**	153	300
49	269.9	300	**67**	428.3	300
50	505.7	300	**68**	636.2	300
51	683	300	**69**	587	150
52	306.2	300	**70**	302.6	150
53	395.4	300	**71**	463.4	150
54	299.6	450	**73***	706	450
55	423	450	**74***	722.8	300
56	550.6	450	**75***	689	600
57	677.6	450	**76***	710.7	600
58	620.7	450	**78***	695.9	750
59	150.8	450	**79***	693.7	900
60	534.3	450	**80***	417	1050
61	520.8	900	**81***	654.1	1050

Table 1. Experimental shot sheet. Shots preceding Shot 42 were used for trial-and-error adjustments to the procedure and not considered in analysis. The missing shot numbers were for control shots in which only the pump or probe beam was fired in vacuum.

*Additional shots performed with a 1000 μm phase plate for the pump beam. Pump energies were increased in comparison to shots done with the default 600 μm phase plate to adjust for increased cross sectional area while attempting to keep the intensities comparable.

Fringe-counting on scattered points	**Fringe-counting on fringe traces**	**Fast Fourier transform (FFT)**
Manual	Semi-automated	Automated
✓ Works for nearly all interferograms. Handles unusual features such as saddle points, islands, and discontinuous fringes.	✓ Works for nearly all interferograms after some manual pre-processing. Handles unusual features such as saddle points, islands, and discontinuous fringes.	× Only works on images with continuous, well-defined fringes. This condition was not met.
× Requires excessive interpolation, which may skew the real data. Choice of interpolation method also affects results due to the smaller sample size.	✓ Uses a reasonable amount of interpolation.	✓ No interpolation
× Data acquisition is very time-consuming.	✓ Relatively quick. Requires manual pre-processing to resize the image and produce synthetic fringe traces using cubic spline fitting.	✓ Very quick

Table 2. Comparison of methods for obtaining phase shift. Fringe-counting on fringe traces is a tradeoff between the speed and accuracy of the FFT method and the flexibility of application of

the fringe-counting on scattered points method. It was chosen for analyzing interferograms with significant fringe shift seen in this experiment.

Natural neighbor	Cubic	Biharmonic spline
Triangulation-based	Triangulation-based	Spline-based
C^1 continuity; C^0 at sample points	C^2 continuity	C^2 continuity
Preserves sampled data points[7]	Preserves sampled data points (triangulation with bicubic spline interpolation)[6]	Preserves sampled data points as closely as possible[6]
Local[8]	Triangulation is always local[8]	By observation, the tension parameter affects interpolation locality
"Performs well even when the data is highly anisotropic," or directional[7] "Perform equally well in clustered and in sparse areas of the given point set"[8]	Produces very smooth surfaces[6]	Produces very smooth surfaces[6]
Fast	Fast	Very computationally intensive[8,9] Not suitable for data sets containing more than a few hundred points[8] Crashed during execution
Density gradient along pump beam height: 6.9×10^{18} cm^{-3} $\leq n_e \leq$ 9.7×10^{18} cm^{-3}	**Density gradient along pump beam height:** 6.9×10^{18} cm^{-3} $\leq n_e \leq$ 9.7×10^{18} cm^{-3}	

Table 3. Comparison of interpolation methods. Natural neighbor and cubic interpolation yielded essentially identical density gradients, although natural neighbor was chosen for the slightly smoother curves it produced.

FIGURES

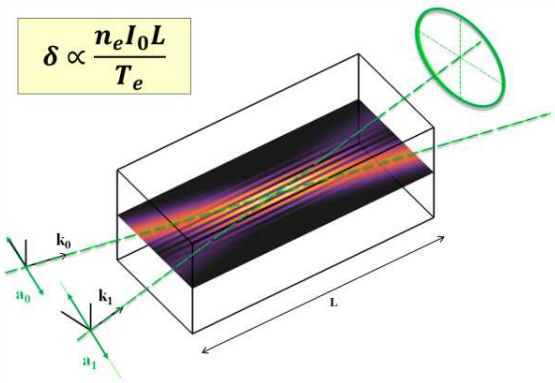

Figure 1.[1] $\mathbf{a_0}$ is the high-energy pump beam and $\mathbf{a_1}$ is the probe beam; both have a wavelength of 1053 nm and intersect in ionized helium plasma at a 27° angle. In the ideal configuration, the pump is horizontally polarized while the probe is initially polarized at 45°. The laser-plasma waveplate acts upon the probe beam.

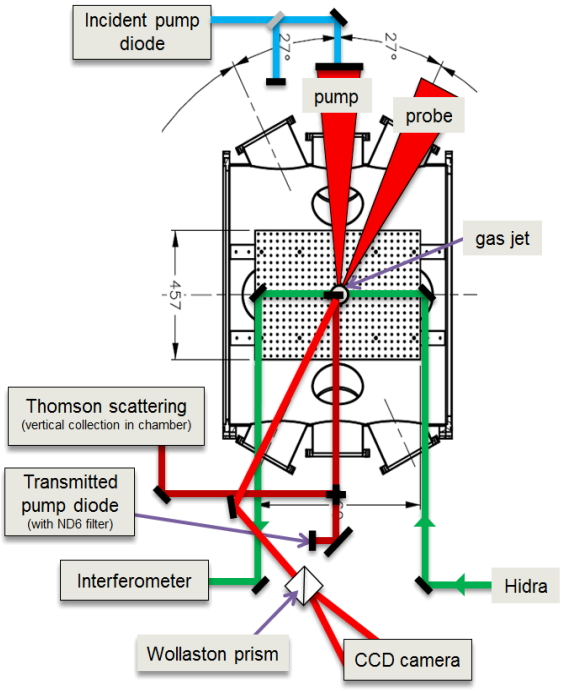

Figure 2.[2] Top-down view of the experimental setup at the Jupiter Laser Facility. Diagnostics are tagged by outlined boxes.

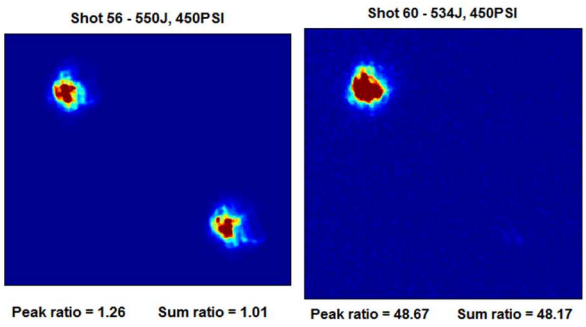

Figure 3.[2] Example images obtained from the probe beam polarization diagnostic. Vertical polarization components are imaged on the upper left side of the CCD plate; horizontal components appear on the bottom left. The image on the left shows polarization with almost equal vertical and horizontal components, while the image on the right shows beam at near-vertical polarization.

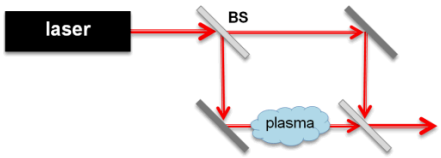

Figure 4. A Mach-Zehnder interferometer. The presence of plasma in one of the legs imparts a phase difference between light travelling along the two legs. No longer lined up, the crests and troughs constructively and destructively interfere to produce a fringe pattern.

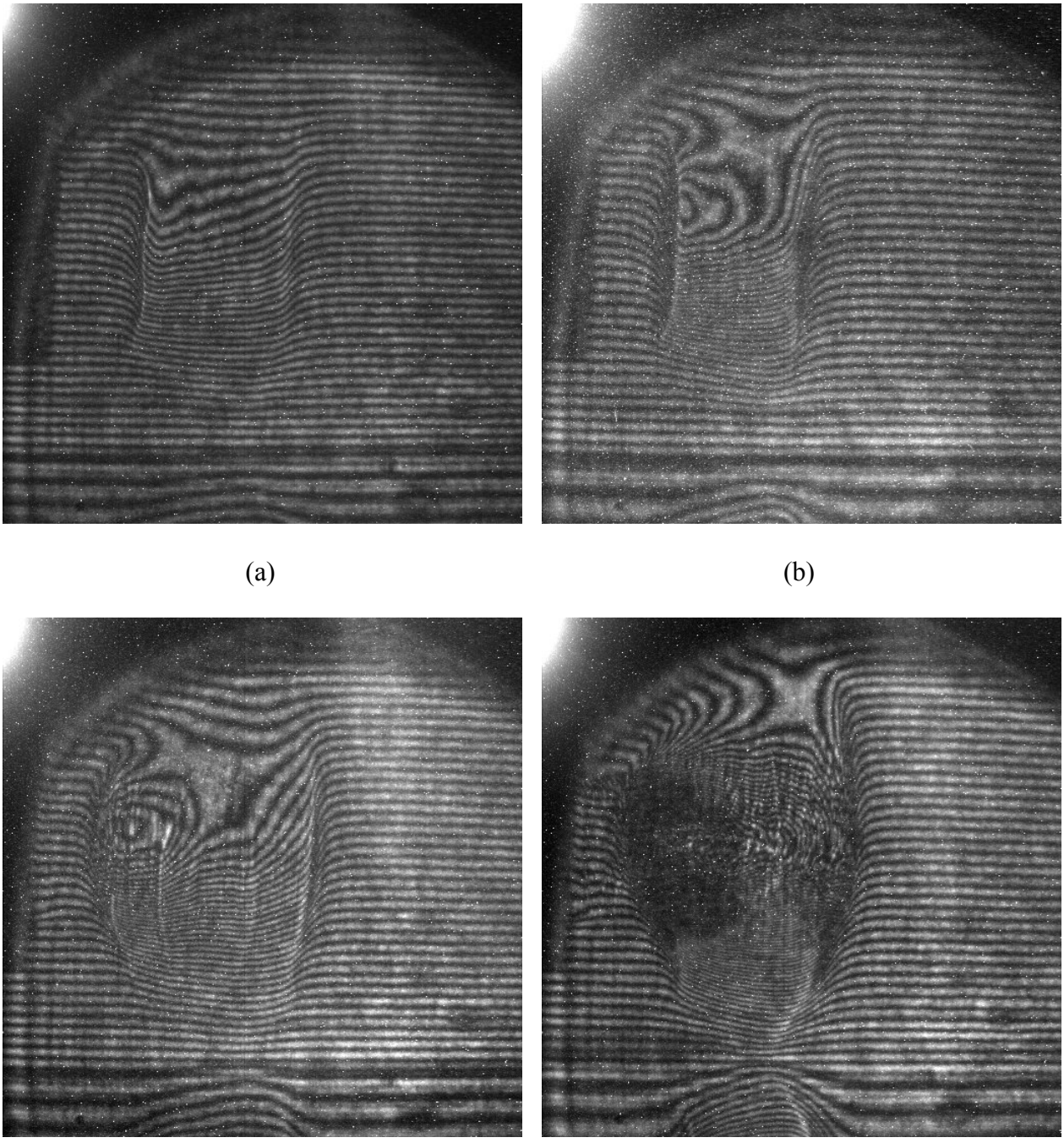

(a) (b)

(c) (d)

Figure 5. Examples of non-ideal features in plasma interferograms, ordered by the effect of increasing intensity, pressure, and interaction length. (a) Discontinuity in the left channel edge in Shot 69 (587 J, 150 psi). This is the result of higher gas density near the gas jet manifested as heavy phase shifting and appeared for nearly all of the shots. It is accounted for in the chosen

analysis technique. (b) Islands and saddle points in Shot 52 (306.2 J, 300 psi). (c) Vertical ridges in Shot 74* (722.8 J, 300 psi). (d) Loss of information at the left channel edge, among other imperfections, in Shot 80* (417 J, 1050 psi).

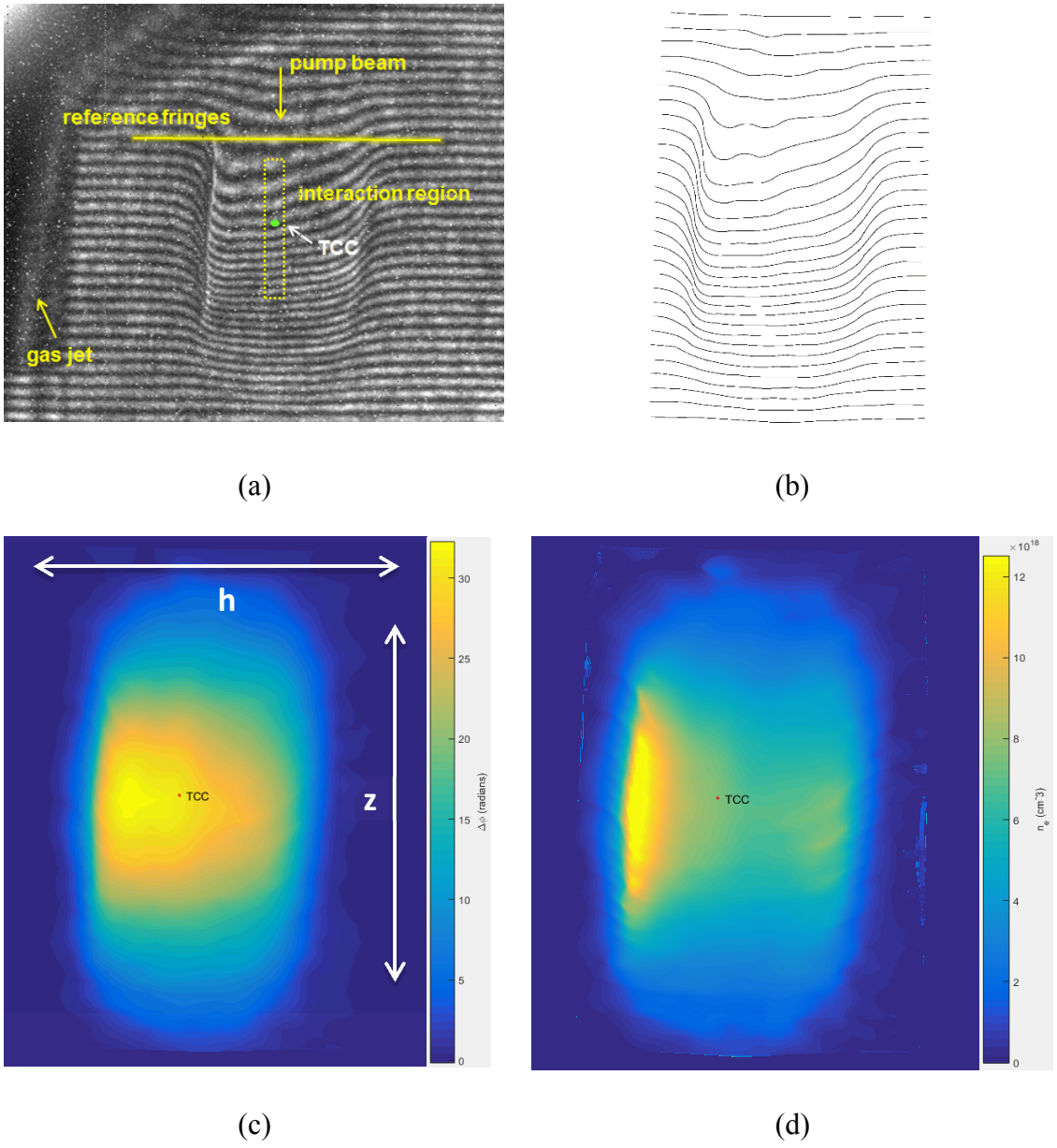

Figure 6. Progression of interferogram analysis for Shot 70 (302.6 J, 150 psi). (a) Raw interferogram. The interaction region is where the pump and probe beams overlap about TCC.

(b) Each fringe was traced in GRIMP using a spline fit. This image is the input to a fringe tracking algorithm that generates a full phase shift map. (c) Phase shift map. (d) Density map.

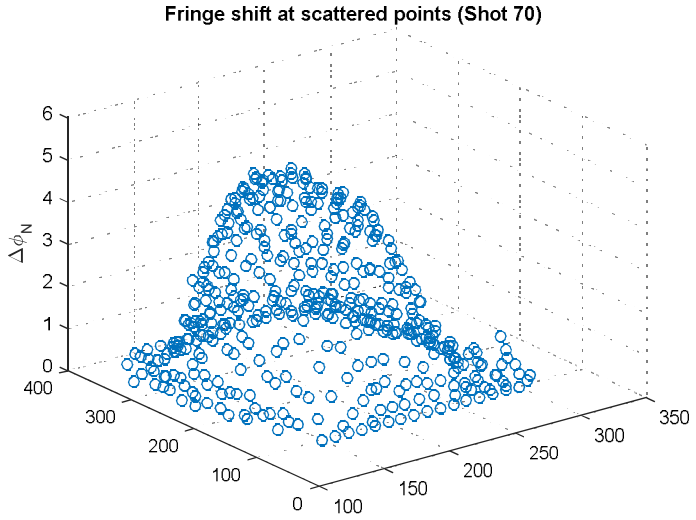

Figure 7. These 400+ points were hand-picked for the fringe-counting on scattered points approach to interferogram analysis.

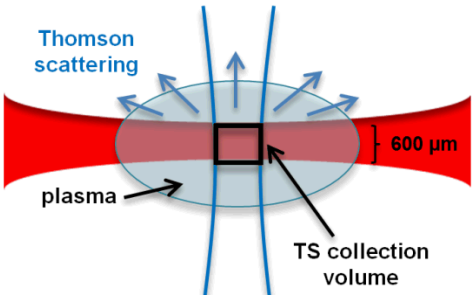

Figure 8. Density along the pump beam height is taken from a lineout of the density map to help constrain the range of possible plasma temperatures from Thomson scattering.

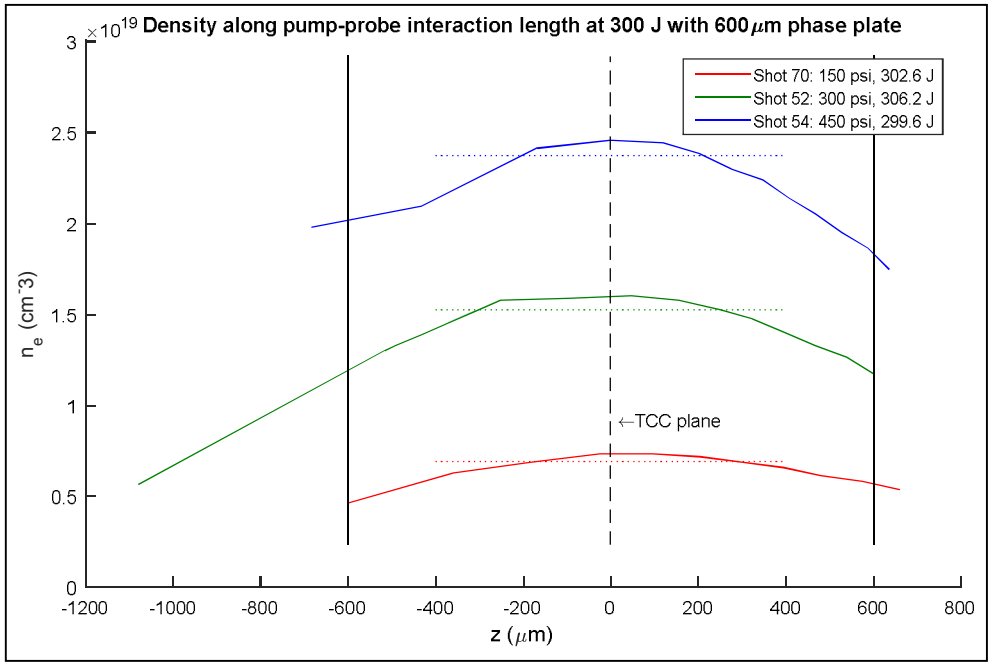

Figure 9. As expected, density increases with increasing gas pressure at a given pump energy; this relation is approximately linear. The dotted lines show the average density for each shot within 400 μm of TCC. There is an estimated ±10% error from the manual location of the fringes.

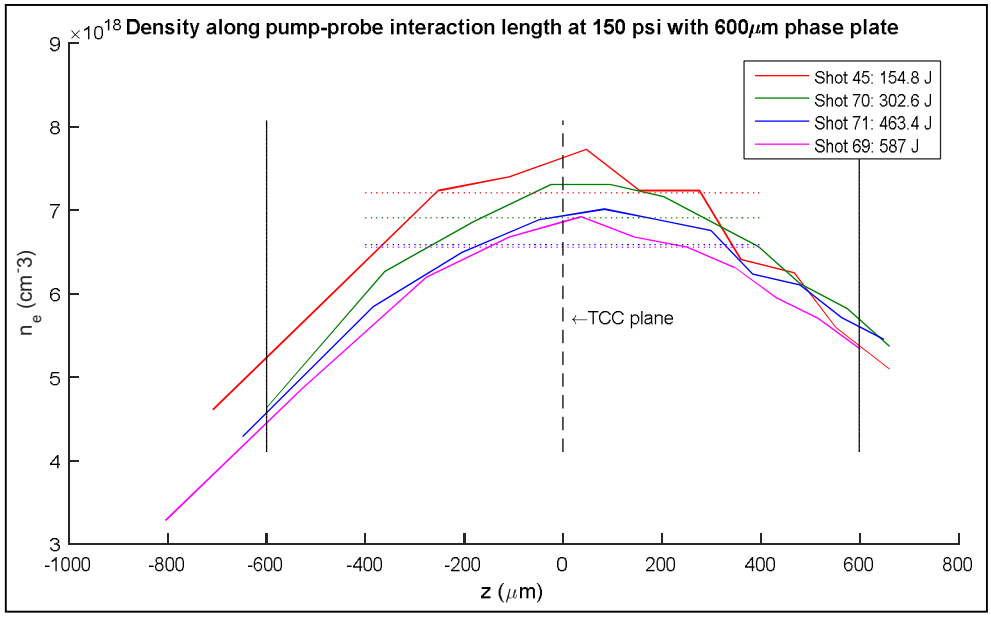

Figure 10. Higher pump energies cause the plasma to expand faster, leading to a decrease in density. However, the effect appears to saturate at high energies. The dotted lines show the average density for each shot within 400 μm of TCC. There is an estimated ±10% error from the manual location of the fringes.

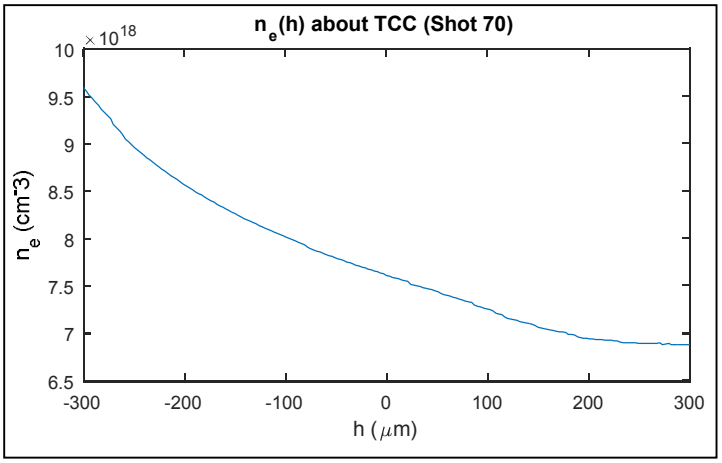

Figure 11. Variation along the h-axis in the plane containing TCC, obtained from a lineout of the density map. This is the most important density gradient for analysis, as it corresponds directly to the collection volume of the Thomson scattering diagnostic: vertically in the target chamber. It is used to constrain temperature information from Thomson scattering.

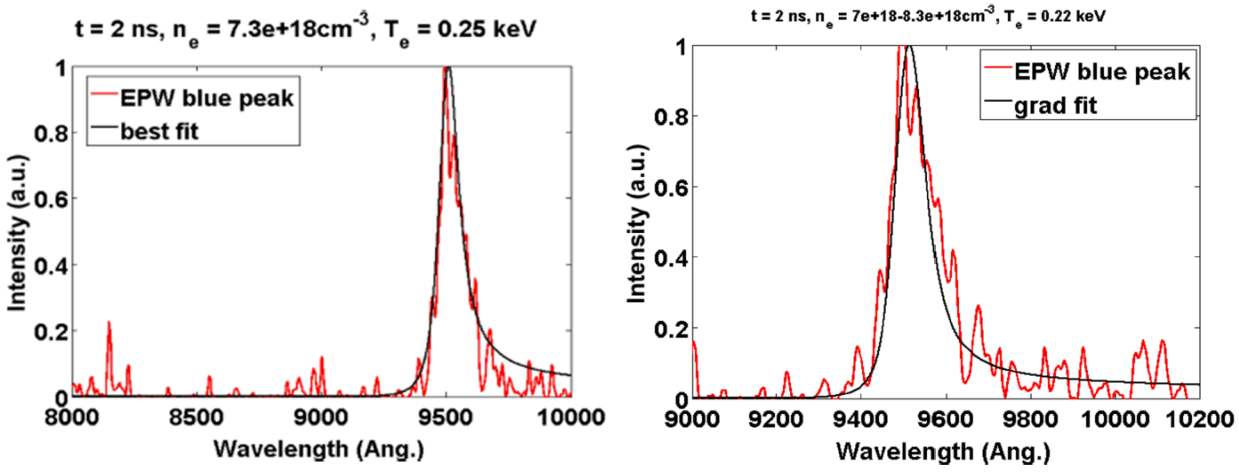

(a) (b)

Figure 12.[5] Fitting experimental Thomson scattering data for Shot 70 by adjusting density and temperature.[3] (a) Best fit achieved using only a single density along the pump beam height. The tails of the two peaks do not agree. (b) The curve of best fit approaches the experimental data much more closely when a density range is taken into account. Notice the resulting lower temperature.

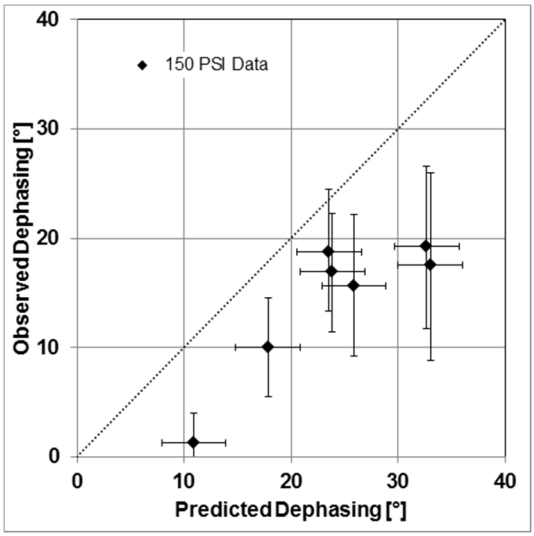

Figure 13.[2] Observed vs. predicted dephasing angles at 150 psi.[2] Despite the offset, the slope is nearly 1, signifying close agreement. The observed dephasing also appears to plateau around 20°; the cause of this is currently under investigation.